Dyes and Pigments 212 (2023) 111148

Contents lists available at ScienceDirect

Dyes and Pigments

journal homepage: www.elsevier.com/locate/dyepig

Sequential recognition capability of a novel flavin-dipicolyl analogue toward zinc and phosphate ion: A model capable of selective recognition of AMP over ADP/ATP

M.S.S. Vinod Mouli, Ashutosh Kumar Mishra *

Department of Chemistry, Indian Institute of Technology, Hyderabad, 502285, India

ARTICLE INFO

Keywords:
Flavin
Dipicolylamine
Zinc
Adenine nucleotide
Phosphate
Quenching

ABSTRACT

A novel flavin-dipicolylamine conjugate was designed for highly selective and sequential recognition of zinc and phosphate ions based on OFF-ON-OFF mode of detection. While lower detection limits were obtained toward zinc ion recognition in the two solvents studied here, different stoichiometric requirement and hence different mode of coordination was also observed and evaluated. Furthermore, the DPF-zinc complex was found to be highly selective for phosphate anion over other anions studied. Variation in the detection limit for phosphate over pyrophosphate was observed making it a model capable of differentiating between AMP from ADP or ATP.

1. Introduction

An insight into the natural system remains the key for the numerous innovative synthetic designs for a range of potential applications [1–3]. The emergence of fluorescent proteins has offered an excellent probe to monitor/track numerous biologically relevant phenomenon such as gene expression, protein localization and biomolecular tracking etc [4–7]. In fact, recently discovered flavin-based fluorescent proteins (FbFPs) has shown an advantage over the green fluorescent protein (GFPs) due to their smaller size and excellent luminescence behavior even in low oxygen environment [8,9]. In the case of FbFPs, a site directed mutagenesis replacing cysteine with alanine moiety near the flavin binding pocket is suggested to render the stable fluorescence behavior [10,11]. Contrary to GFPs, which show diminished emission under low oxygen environment, FbFPs could be a suitable tracker for investigating anaerobic phenomenon as well such as tumor hypoxia, cerebral ischemia, pathogenesis to name a few [11].

Now, the core structural unit in FbFPs responsible for the luminescence behavior is the tricyclic fused isoalloxazine ring present in the flavin cofactor (Fig. 1a). Notably, variation in luminescence behavior of the flavin has been reported in presence of suitable donor moiety with feasible charge transfer process both in natural [12–14] and synthetic model systems [15–29]. Notably, the suitable spatial orientation of the adenine moiety with respect to isoalloxazine ring in flavin adenine dinucleotide (FAD) is reportedly undergoes a photoinduced electron transfer process thereby regulating the flavin emission spectra [30–32]. Such observations can be harnessed for designing the novel models for sensing based applications. In fact, a zinc complex was reported to block the charge transfer pathway via coordinating to the phosphate group of the FAD, resulting the enhanced emission for selective detection of the FAD [33]. Despite the excellent luminescence properties of the flavin entity, limited synthetic models around flavin core have been reported for analytical sensing purposes [34–37].

Interested in modulating the structural and functional nature of flavin via metal ion interaction [38–41], we decided to design and develop a flavin model as fluorescence probe for sequential recognition of the zinc and the phosphate ions. While on one hand, the otherwise essential zinc ion is a biologically essential entity, any disruption in the zinc homeostasis is reportedly associated with various neurological and growth factors related issues such as protein deregulation [42,43], synaptic plasticity [44,45], cerebral ischemia, epilepsy and Alzheimer's disease [46–48], diabetes [49–51] and prostate malignancy [52–54]. On other hand, selective detection of phosphate is also deemed essential due to its involvement in key biochemical phenomenon associated with bio-energetic or post-translational protein modifications. Various synthetic models have been reported as efficient probes for both zinc ion as well as phosphate anion. Interestingly, few of these synthetic models involves design around zinc complexes for efficient phosphate sensing [55,56]. Converging the key structural constituents of these probes could lead to a simple yet elegant singular model for the sequential zinc

* Corresponding author.
E-mail address: akm@chy.iith.ac.in (A.K. Mishra).

https://doi.org/10.1016/j.dyepig.2023.111148
Received 31 December 2022; Received in revised form 1 February 2023; Accepted 1 February 2023
Available online 4 February 2023

and phosphate sensing.

In this context, our earlier work involves selective positioning of the metal ion within the flavin framework for the generation of polymeric motif and their facile transfer onto a surface as well as for modulating the catalytic behavior toward aerobic sulphoxidation reactions [38–41]. Here, our efforts with the synthesis and structural characterization of a novel flavin analogue (**DPF**) having dipicolylamine pendant is achieved and investigated for sequential detection of zinc metal and phosphate anion. Incorporating DPA (dipicolylamine) pendant at N10 position of the flavin moiety would provide a smooth access for the zinc ion coordination, also being an electron rich species can undergo effective charge transport process resulting in the emission quenching of the flavin moiety.

With this design strategy in mind, we have synthesized and characterized 10-(2-(bis(pyridin-2-ylmethyl)amino)isoalloxazine as shown in Fig. 1c. Further photophysical studies have revealed the selective and sequential detection capabilities of the **DPF** as fluorescent probe for zinc and phosphate ions. In-depth investigation was performed to understand the substantial enhancement in the emission spectra with the addition of zinc ion when methanol was used as solvent compared to DMSO. As suggested by the Job's plot analysis, the possibility of having two different stoichiometric species in the two solvents used for this study might be responsible for the different level of the operational charge transfer process between the DPA and flavin moiety. This simple model was found to be capable of distinguishing between Adenine monophosphate (AMP) from its di- or tri-phosphate analogues (ADP or ATP) which is discussed in this manuscript.

2. Experimental section

2.1. Materials and measurements

All chemicals and reagents were purchased from Sisco Research Laboratories Pvt. Ltd.(SRL) - India and Sigma-Aldrich and used without purification. Nuclear magnetic resonance spectra were collected using Bruker DRX-400 spectrometer at ambient temperature. ^{13}C NMR spectra were obtained at 100 MHz and ^{1}H NMR spectra were obtained at 400 MHz. Resonances are reported in parts per million (ppm) and coupling constants (*J*) are reported in hertz (Hz). High resolution mass spectra were obtained by Electron Spray Ionization method (ESI) using Agilent QTOF 6538. UV–Visible spectral measurements were obtained from JASCO spectrophotometer V730 in the range of 200–700 nm at 25 °C. Fluorescence measurements were taken from JASCO Spectrofluorometer FP-8300 in the range of 450 nm–800 nm at 25 °C. Infrared measurements were done using Bruker ALPHA FT-IR in the range 4000 cm^{-1} to 500 cm^{-1} at 25 °C.

2.2. Synthesis of DPF

DPF is synthesized by following the modified reported procedure as discussed below [15–29,38–41,57]. A schematic representation of the synthesis is represented in Scheme 1.

2.2.1. N1-(2-nitrophenyl)ethane-1,2-diamine (2)

To 100 mL RB containing 2-Nitrochlorobenzene **1** (1 g, 6.35 mmol) added ethane-1,2-diamine (20 mL) followed by addition of K_2CO_3 (0.87 g, 6.35 mmol). Reaction mixture was kept for reflux for 12 h under inert atmosphere. After completion of reaction the contents were extracted with chloroform (150 × 3 mL) from brine (100 mL). Organic layer was dried using anhydrous Na_2SO_4, filtered and evaporated, to it added methanol followed by addition of Conc. HCl (2 mL), allowed to stand at 0 °C for 1 day. Yellow crystals of hydrochloride salt of **2** formed was suction filtered and washed with cold methanol. Further base extraction using chloroform (150 × 2 mL) from 0.1 M NaOH (100 mL) was done followed by washing with brine (100 mL). Dried organic layer using anhydrous Na_2SO_4, filtered and evaporated under reduced pressure to give **2** as yellow oil. Yield 80%. ^{1}H NMR (400 MHz, $CDCl_3$): δ 8.26 (s, 1H), 8.17 (dd, 1H, *J* = 8.6, 1.2 Hz), 7.44 (dd, 1H, *J* = 11.3, 4.2 Hz), 6.88 (d, 1H, *J* = 8.6 Hz), 6.65 (t, 1H, *J* = 7.7 Hz), 3.39 (dd, 2H, *J* = 11.7, 5.8 Hz), 3.06 (t, 2H, *J* = 6 Hz), 1.44 (s, 2H). ^{13}C NMR (100 MHz, MeOD): δ 146.35, 137.50, 133.68, 127.70, 116.80, 115.05, 43.68, 40.32. FT-IR (cm^{-1}): 3368, 2924, 2860, 1614, 1567, 1505, 1416, 1346, 1236, 1149, 1030, 942, 853, 739. HRMS (ESI) *m/z*: $[M+H]^+$ calcd for $C_8H_{12}N_3O_2$: 182.0924 Found 182.0924.

2.2.2. N1-(2-nitrophenyl)-N2,N2-bis(pyridin-2-ylmethyl)ethane-1,2-diamine (3)

To 25 mL RB flask added **2** (0.5 g, 2.3 mmol) followed by addition of 1,2-dichloroethane (DCE, 15 mL). 2-Pyridine carboxyaldehyde (0.739 g, 6.9 mmol) was added to the reaction mixture and continued stirring for 24 h under inert atmosphere. The reaction was then stopped, evaporated DCE under reduced pressure and silica gel column chromatography was done by gradient elution with DCM and methanol (up to 5%) to give **3** as thick yellow oily liquid. Yield 50%. ^{1}H NMR (400 MHz, $CDCl_3$): δ 8.5 (t, 1H, *J* =1.32 Hz), 8.49 (t, 1H, *J* = 1.3 Hz), 8.46 (s, 1H), 8.17 (dd, 1H, *J* = 8.6, 1.6 Hz), 7.68 (m, 4H), 7.37 (ddd, 1H, *J* = 8.4, 7, 1.3 Hz), 7.14 (ddd, 2H, *J* = 6.1, 5, 2.5 Hz), 6.72 (dd, 1H, *J* = 8.6, 0.8 Hz), 6.62 (ddd, 1H, *J* = 8.4, 6.9, 1.2 Hz), 3.89 (s, 4H), 3.38 (dd, 2H, *J* = 11.3, 4.9 Hz), 2.93 (t, 2H, *J* = 5.88 Hz). ^{13}C NMR (100 MHz, $CDCl_3$): δ 158.9, 148.89, 145.24, 136.79, 136.14, 131.9, 126.84, 123.28, 122.24, 115.13, 113.99, 60.5, 52.07, 40.17. FT-IR (cm^{-1}): 3365, 2836, 1613, 1570, 1507, 1423, 1349, 1242, 1148, 1041, 851, 742. HRMS (ESI) *m/z*: $[M+H]^+$ calcd for $C_{20}H_{21}N_5O_2$: 364.1768 Found 364.1769.

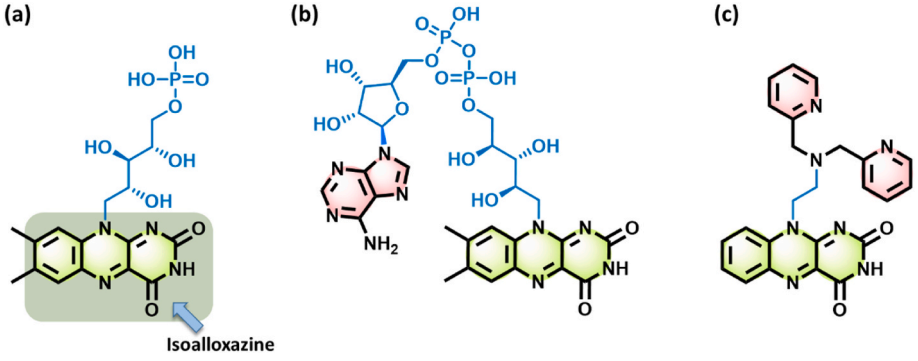

Fig. 1. Representation of the chemical structure of the naturally occurring flavin mononucleotide FMN (a), flavin adenine dinucleotide FAD (b) and our designed flavin analogue **DPF** (c).

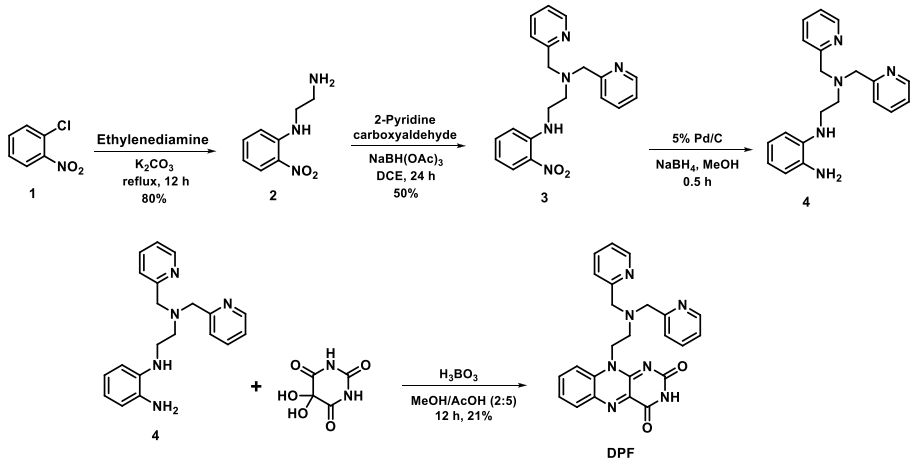

Scheme 1. Synthesis of **DPF** analogue.

2.2.3. *N1-(2-(bis(pyridin-2-ylmethyl)amino)ethyl)benzene-1,2-diamine (4)*

To **3** (120 mg, 0.33 mmol) taken in 25 mL RB flask added methanol (5 mL) followed by addition of Pd/C (30 mg) and started stirring at room temperature. Sodium borohydride (50 mg, 1.32 mmol) in was added in two portions for 10 min. Continued stirring under empty balloon for 30 min. After completion of reaction monitored by TLC, the reaction contents were suction filtered to remove Pd/C, washed with chloroform and extracted filtrate with DCM (150 × 2 mL) from water (100 mL). Dried the organic portion with Na_2SO_4 and concentrated under reduced pressure to give diamine as dark yellow oil which was used for next reaction without any further purification.

2.2.4. *10-(2-(bis(pyridin-2-ylmethyl)amino)isoalloxazine (DPF)*

To Alloxan monohydrate (53 mg, 0.33 mmol) and boric acid (20.5 mg, 0.33 mmol) taken in 25 mL RB flask added 2 ml methanol. Diamine **4** dissolved in glacial acetic acid (5 mL) is then added to reaction mixture dropwise for 30 min. Stirring is continued at room temperature under inert atmosphere for 12 h. After completion of reaction, acetic acid is evaporated under reduced pressure and silica gel column chromatography is done by gradient elution with chloroform and methanol (up to 15%) to give **DPF** as yellow solid. Yield 21%, MP: 206–210 °C. ^{1}H NMR (400 MHz, DMSO-d_6): δ 11.35 (s, 1H), 8.39 (d, 2H, J = 4.2 Hz), 8.12 (d, 1H, J = 8.1 Hz), 7.88 (d, 1H, J = 8.7 Hz), 7.77 (t, 1H, J = 7.7 Hz), 7.6 (t, 1H, J = 7.6 Hz), 7.54 (t, 2H, J = 7.6 Hz), 7.15 (t, 4H, J = 8.5 Hz), 4.81 (s, 2H), 3.83 (s, 4H), 2.96 (t, 2H, J = 5.9 Hz). ^{13}C NMR (100 MHz, DMSO-d_6): δ 159.62, 158.58, 155.27, 150.27, 148.62, 136.2, 134.79, 134.65, 132.74, 131.68, 125.84, 124.57, 122.44, 122.01, 116.59, 59.68, 49.37, 42.25. FT-IR (cm^{-1}): 3025, 2818, 2340, 1669, 1544, 1428, 1245, 1112, 827, 756. HRMS (ESI) *m/z*: $[M+H]^+$ calcd for $C_{24}H_{21}N_7O_2$: 440.1829 Found 440.1835.

2.3. *UV–vis absorption and fluorescence spectroscopic methods*

All the spectral measurements were done at 25 °C. Stock solution of **DPF** was prepared in HPLC grade DMSO whereas stock solution of metal salts and nucleotides were prepared in HPLC grade water. For screening metal ions corresponding nitrate salts were used- $NaNO_3$, KNO_3, $Mg(NO_3)_2.6H_2O$, $Ca(NO_3)_2.4H_2O$, $Sr(NO_3)_2$, $Ba(NO_3)_2$, $Cr(NO_3)_3.9H_2O$, $Fe(NO_3)_3.9H_2O$, $Co(NO_3)_2.6H_2O$, $Ni(NO_3)_2.6H_2O$, $Cu(NO_3)_2.3H_2O$, $AgNO_3$, $Zn(NO_3)_2.6H_2O$, $Cd(NO_3)_2.4H_2O$, $Pb(NO_3)_2$ and $Hg(NO_3)_2.H_2O$. For screening anions corresponding sodium salts are used (for phosphate, potassium salt is used) – NaF, NaCl, NaBr, NaI, $NaNO_3$, Na_2CO_3, $NaHCO_3$, K_3PO_4, $Na_4P_2O_7$, NaOAc, Na_2SO_4, Na_3(Citrate). Adenine nucleotides (AMP, ADP, ATP) are used as their corresponding sodium salts. Appropriate amount of metal salt was added to **DPF** and incubated for 5 min before recording the spectra. Fluorescence quantum yields (Φ) were determined by using Coumarin 153 as standard with a known quantum yield of 0.544 in ethanol [58].

3. Result and discussion

In order to understand the photoluminescence behavior of the **DPF** moiety, absorption spectrum was recorded at room temperature using 50 μM solution in DMSO and compared with 10-propylflavin (**PF**) (without the dipicolylamine pendant) [38]. As shown in Fig. 2a, both the **DPF** and **PF** displays three characteristic absorption bands in DMSO with wavelength maxima at around 264, 333 and 438 nm for **DPF** and 268, 331 and 434 nm for **PF**, which are typically assigned to the π-π* transition of the isoalloxazine entity [12–14,34–37]. Though a subtle shift in the higher energy band of **DPF** (438 nm) was observed when compared to **PF** (434 nm), no significant difference was observed in the absorption spectra between the two flavin analogues.

As anticipated, a substantial decrease in the emission spectra was observed for **DPF** as compared to **PF** moiety. As shown in Fig. 2b, the emission spectra of **DPF** and **PF** when excited at 438 nm and 434 nm respectively, displays a strong emission band for **PF** at around 527 nm, typically assigned to the emission spectra of the isoalloxazine ring. On the other hand, the DPF moiety show almost a flat spectrum indicating the efficient excited state charge transfer process involving the electron rich dipicolylamine unit and electron deficient flavin unit.

A careful screening of the emission spectra for **DPF** in presence of a variety of metal ions was performed using 1:1 metal to **DPF** ratio to investigate the selectivity of the **DPF** toward the zinc ion (Fig. 3). Considering the significant role of solvent in affecting the overall coordination sphere, connectivity and the resultant architecture [59,60]; we decided to perform the investigation in two different solvents-a polar aprotic (DMSO) and a polar protic (methanol) solvent. Analysis of the emission spectra in presence of various metal nitrates revealed a high selectivity for zinc ion over other metal ions in both the solvents studied here selectively. A slight enhancement in the emission intensity was also observed for cadmium followed by mercury (belonging to same group) as well, however insignificant when compared to the zinc ion [61–65].

More interestingly, a significant difference in the emission enhancement was observed for the different solvents used. While both the solvents support the selective recognition of zinc ion, a substantial 18-fold increase in the emission intensity was observed in methanol as compared to 7.5-fold increase in DMSO as solvent (Fig. 4). While it is quite evident that the zinc coordination to dipicolylamine appendage can successfully block the charge transfer process in **DPF** resulting in resurgence of the isoalloxazine emission; possibility of formation of different metalated species under different solvent conditions cannot be

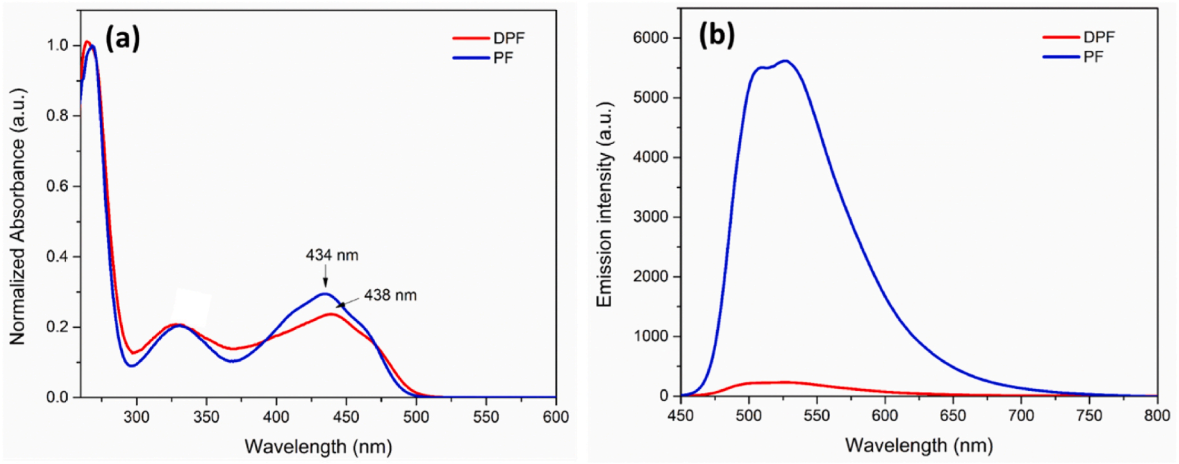

Fig. 2. (a) UV–Vis and (b) fluorescence spectra of **DPF** and **PF** using 50 μM concentration in DMSO.

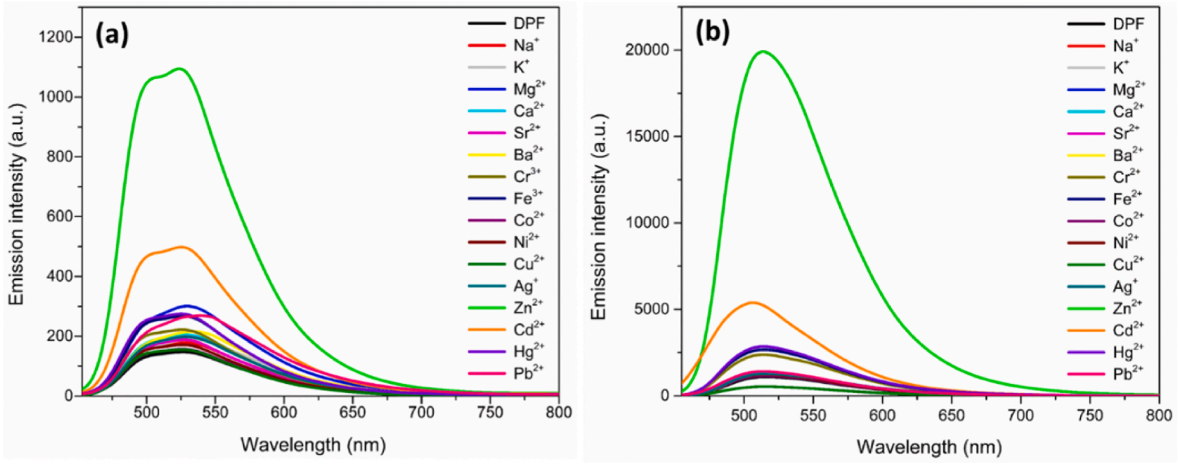

Fig. 3. Screening of emission spectra of the **DPF** (50 μM) against different metal ions using equimolar solution in (a) DMSO and (b) methanol.

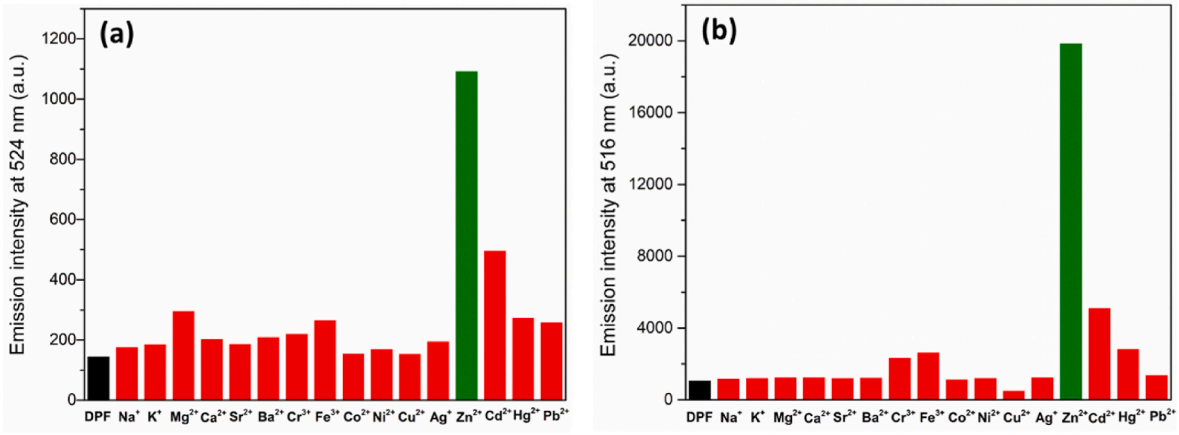

Fig. 4. Bar graph representation of the emission intensity of the **DPF** moiety in the presence of different metal ions in (a) DMSO and (b) Methanol.

ruled out.

To understand the stoichiometric requirement for the **DPF** zinc complexation in the two solvents used in this study, the fluorescence titration studies were performed with added zinc ion in DMSO and methanol as solvents (Figs. 5a and 6a). Job's plot analysis of the fluorescence titration studies displays the maximum emission intensity at approximately 0.49 and 0.32 mole fraction of **DPF** in DMSO and methanol respectively (Figs. 5b and 6b). This is indicative of 1:1 stoichiometry between **DPF** and zinc ion in case of DMSO, while 2:1 stoichiometry was observed between **DPF** and zinc in case where methanol is used as solvent as shown in Scheme 2. Furthermore, the binding affinity of the **DPF** toward zinc ion was also determined using Benesi-

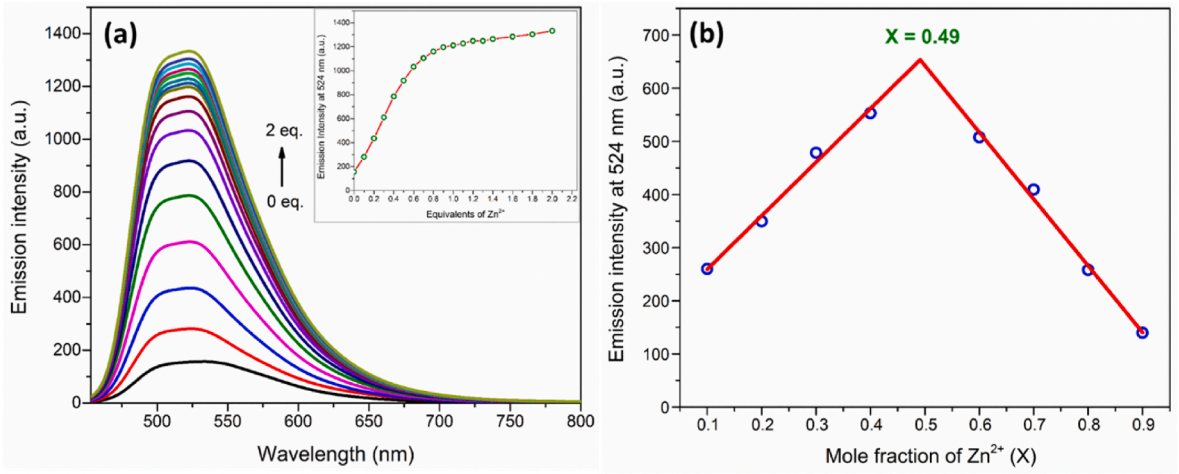

Fig. 5. (a) Representation of the **DPF** emission (50 μM) with the increasing concentration of the Zn^{2+} in DMSO. Inset displays a derivative plot of the emission intensity of **DPF** against the equivalents of Zn^{2+} ion in DMSO. (b) Representation of the Job's plot as determined in DMSO.

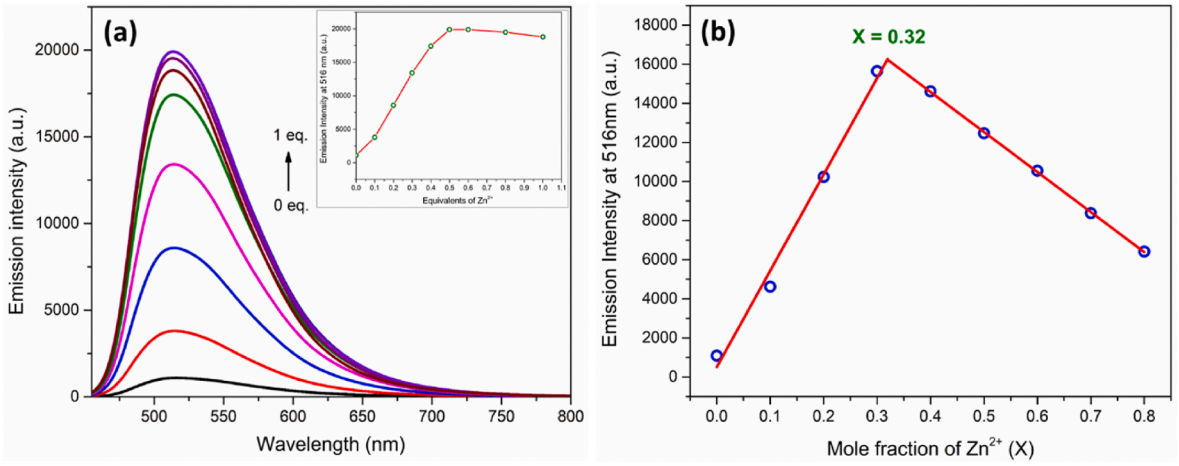

Fig. 6. (a) Representation of the **DPF** emission spectra (50 μM) with increasing concentration of Zn^{2+} in methanol. Inset displays a derivative plot of the emission intensity of **DPF** against the equivalents of Zn^{2+} ion in methanol. (b) Representation of the Job's plot as determined in methanol.

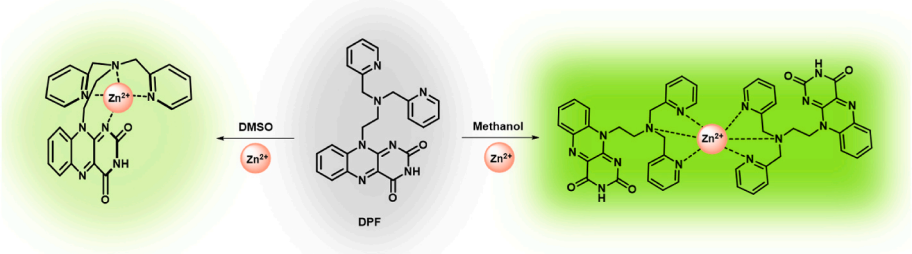

Scheme 2. A proposed model for zinc ion complexation with the **DPF** moiety in DMSO and methanol.

Hildebrand equation considering the stoichiometric ratio obtained in DMSO and methanol from the job's plot analysis [66,67]. A higher binding affinity was observed for **DPF** and zinc ion as suggested from the binding constant values determined in DMSO and methanol ($(1.237 \pm 0.034) \times 10^4\ M^{-1}$ and $(1.713 \pm 0.299) \times 10^2\ M^{-2}$ respectively).

Corroboratory evidence was also obtained with the quantum yield calculations performed in DMSO and methanol solvent as shown in Table S1. While **DPF** alone shows a significantly low quantum yield value of 0.014 (in DMSO) and 0.003 (in methanol) as compared to **PF** alone (0.23 in methanol); an increased quantum yield value was observed for the DPF-Zinc conjugate. Slightly, better quantum yield was obtained for **DPF-Zn** conjugate in methanol (0.152) as compared to that in DMSO (0.119). In addition, a linear relationship between the emission intensity of the **DPF** and the zinc ion (over a concentration range of 0–30 μM) was observed as shown in Fig. S2. The calculated detection limit for zinc ion using **DPF** was found to be 236.8 nM and 4.022 nM in DMSO and methanol respectively [68]. While a better detection limit was obtained in case of methanol as solvent; the LOD obtained in both the solvents used in this study was found to be significantly lower than the concentration denoted for the chronic zinc ion contamination by the US Environment and Protection Agency (USEPA), (>1.84 μM) [69].

As shown in Fig. 7, the interference of other metal ions over zinc ion

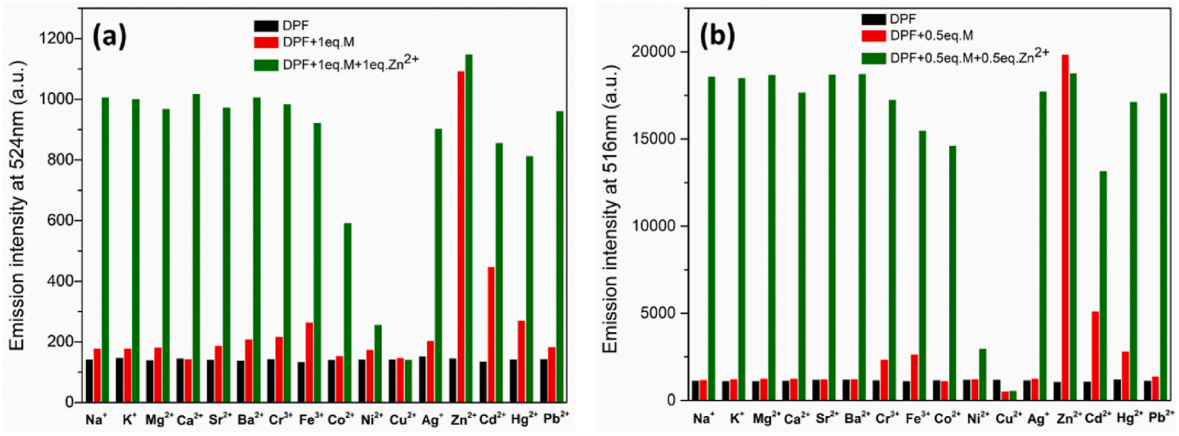

Fig. 7. A bar graph representation for the metal ion interference using **DPF** probe (50 μM) towards zinc ion selectivity in (a) DMSO and (b) Methanol.

selectivity was also investigated. While the emission profile remains unperturbed in presence of most of the metal ions used in this study including the biologically abundant ones (Na^+, K^+, Ca^{2+}, Mg^{2+}); strong inference was observed in case of Ni^{2+}, Cu^{2+}, which are known for their fluorescence quenching behavior [70–72]. Notably, the subtle enhancement was observed in presence of Cd^{2+}, though to a smaller extent. Similar to our other observations here, a more pronounced effect was observed with the methanol as compared to the DMSO as solvent used for the emission studies.

To investigate the sequential detection mode of **DPF**, the emission studies were performed by adding two equivalents of various anions to the methanolic solution of **DPF-Zn** complex. While insignificant change in the emission spectra was observed with the addition of the F^-, Cl^-, Br^-, I^-, NO_3^-, CO_3^{2-}, HCO_3^{2-}, CH_3COO^-, SO_4^{2-} and citrates anions; a substantial thirteen-fold decrease in the emission intensity was observed for PO_4^{3-} anion suggesting high selectivity towards the phosphate anion over other anions as shown in Fig. 8a. Interestingly, only two-fold decrease in the emission intensity was observed for the addition of pyrophosphate species. Possibly the varying strength of the coordinating anions to the zinc center might be responsible for reorganization of the coordination sphere around zinc center thereby activating the charge transfer process between the isoalloxazine and dipicolyl moiety to a different extent and hence the observed variation in the emission intensity.

Furthermore, the observed selectivity for phosphate over pyrophosphate anion has prompted us to the investigate the **DPF-Zn** probe for potential screening of adenine monophosphates (AMP) over adenine diphosphate (ADP) and adenine triphosphate (ATP). The emission spectra as shown in Fig. 8b, reveals approximately eleven-fold decrease in the emission intensity with the addition of 1 equivalent of the AMP; as compared to the subtle decrease (approx. two-fold) with the addition of ADP or ATP.

4. Conclusion

In summary, a flavin-dipicolyl (**DPF**) conjugate was designed and developed as efficient fluorescent probe for the sequential and selective detection of the zinc ion and phosphate anion in an OFF-ON-OFF mode. Interesting variation in the detection limit was observed for the **DPF** conjugate in two different solvents (DMSO and methanol), possibly resulting from the different stoichiometric requirement for complexation as suggested by Job's plot analysis. A lower limit of detection (4.02 nM) was obtained in methanol towards zinc ion which is within the permissible limit as suggested by USEPA. This **DPF** model has further shown sequential selectivity capability towards phosphate anion, which was utilized to differentiate between AMP over ADP and ATP.

CRediT authorship contribution statement

M.S.S. Vinod Mouli: Both the authors contributed for the inception of idea to writing the manuscript. has performed all the experimental work and collected the, Data curation, Formal analysis, and manuscript writing was done by both the authors. **Ashutosh Kumar Mishra:** Both the authors contributed for the inception of idea to writing the

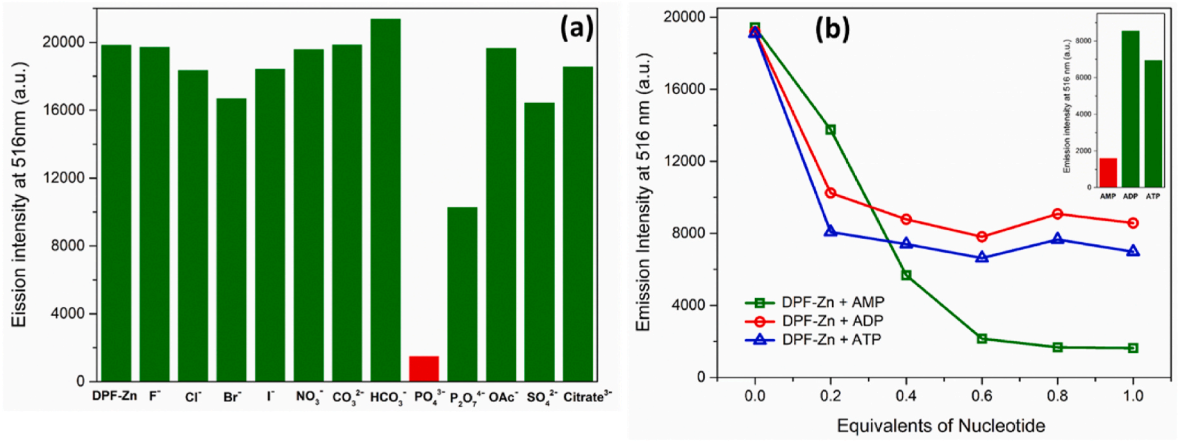

Fig. 8. (a) Representation of plot displaying selectivity of **DPF-Zn** towards phosphate anion over the other anions studied in methanol. (b) Representation of plot displaying emission intensity with equivalents of adenine nucleotides, the inset represents a bar graph for emission intensity at one equivalents of nucleotides.

manuscript. has performed all the experimental work and collected the, Data curation, Formal analysis, and manuscript writing was done by both the authors.

Declaration of competing interest

The authors declare that they have no known competing financial interests or personal relationships that could have appeared to influence the work reported in this paper.

Data availability

Data is given in the supporting information section

Acknowledgements

MSSVM thanks MHRD for the fellowship. AKM thanks Science and Engineering Research Board (SERB) India for the research funding (CRG/2022/006706). Both the authors thank Indian Institute of Technology Hyderabad for providing the necessary infrastructure and the instrumentation facilities.

Appendix A. Supplementary data

Supplementary data to this article can be found online at https://doi.org/10.1016/j.dyepig.2023.111148.

References

[1] Guindani C, da Silva LC, Cao S, Ivanov T, Landfester K. Synthetic cells: from simple bio-inspired modules to sophisticated integrated systems. Angew Chem Int Ed 2022;61:e202110855. https://doi.org/10.1002/anie.202110855.
[2] Xu T, Xu LP, Zhang X, Wang S. Bioinspired superwettable micropatterns for biosensing. Chem Soc Rev 2019;48:3153–65. https://doi.org/10.1039/C8CS00915E.
[3] Das A, Hessin C, Ren Y, Desage-El Murr M. Biological concepts for catalysis and reactivity: empowering bioinspiration. Chem Soc Rev 2020;49:8840–67. https://doi.org/10.1039/D0CS00914H.
[4] Zimmer M. Green fluorescent protein (GFP): applications, structure, and related photophysical behavior. Chem Rev 2002;102:759–82. https://doi.org/10.1021/cr010142r.
[5] Kremers GJ, Gilbert SG, Cranfill PJ, Davidson MW, Piston DW. Fluorescent proteins at a glance. J Cell Sci 2011;124:157–60. https://doi.org/10.1242/jcs.072744.
[6] Chudakov DM, Matz MV, Lukyanov S, Lukyanov KA. Fluorescent proteins and their applications in imaging living cells and tissues. Physiol Rev 2010;90:1103–63. https://doi.org/10.1152/physrev.00038.2009.
[7] Shaner NC, Patterson GH, Davidson MW. Advances in fluorescent protein technology. J Cell Sci 2007;120:4247–60. https://doi.org/10.1242/jcs.005801.
[8] Elgamoudi BA, Ketley JM. Lighting up my life: a LOV-based fluorescent reporter for *Campylobacter jejuni*. Res Microbiol 2018;169:108–14. https://doi.org/10.1016/j.resmic.2017.10.003.
[9] Losi A, Gardner KH, Möglich A. Blue-Light receptors for optogenetics. Chem Rev 2018;118:10659–709. https://doi.org/10.1021/acs.chemrev.8b00163.
[10] Buckley AM, Petersen J, Roe AJ, Douce GR, Christie JM. LOV-based reporters for fluorescence imaging. Curr Opin Chem Biol 2015;27:39–45. https://doi.org/10.1016/j.cbpa.2015.05.011.
[11] Mukherjee A, Schroeder CM. Flavin-based fluorescent proteins: emerging paradigms in biological imaging. Curr Opin Biotechnol 2015;31:16–23. https://doi.org/10.1016/j.copbio.2014.07.010.
[12] Dozova N, Lacombat F, Bou-Nader C, Hamdane D, Plaza P. Ultrafast photoinduced flavin dynamics in the unusual active site of the tRNA methyltransferase TrmFO. Phys Chem Chem Phys 2019;21:8743–56. https://doi.org/10.1039/C8CP06072J.
[13] Iuliano JN, Hall CR, Green D, Jones GA, Lukacs A, Illarionov B, Bacher A, Fischer M, French JB, Tonge PJ, Meech SR. Excited state vibrations of isotopically labeled FMN free and bound to a light–oxygen–voltage (LOV) protein. J Phys Chem B 2020;124:7152–65. https://doi.org/10.1021/acs.jpcb.0c04943.
[14] Brazard J, Usman A, Lacombat F, Ley C, Martin MM, Plaza P. New insights into the ultrafast photophysics of oxidized and reduced FAD in solution. J Phys Chem A 2011;115:3251–62. https://doi.org/10.1021/jp110741y.
[15] Hermann DT, Schindler AC, Polborn K, Gompper R, Stark S, Parusel ABJ, Grabner G, Köhler G. Synthesis, spectroscopy, and semiempirical study of a novel porphyrin–flavin dyad. Chem Eur J 1999;5:3208–20. https://doi.org/10.1002/(SICI)1521-3765(19991105)5:11<3208::AID-CHEM3208>3.0.CO;2-O.
[16] Gouloumis A, Rahman GMA, Abel J, de la Torre G, Vázquez P, Echegoyen L, Guldi DM, Torres T. Flavin core as electron acceptor component in a zinc(II)-Phthalocyanine-Based dyad. Aust J Chem 2008;61:256–61. https://doi.org/10.1071/CH08006.
[17] Paul S, Meng L, Berger S, Grampp G, Matysik J, Wang X. The flavin–tryptophan dyad F10T as a cryptochrome model compound: synthesis and photochemistry. ChemPhotoChem 2017;1:12–6. https://doi.org/10.1002/cptc.201600025.
[18] König B, Pelka M, Zieg H, Ritter T, Bouas-Laurent H, Bonneau R, Desvergne JP. Photoinduced electron transfer in a phenothiazine-riboflavin dyad assembled by zinc-imide coordination in water. J Am Chem Soc 1999;121:1681–7. https://doi.org/10.1021/ja9836693.
[19] Shirdel J, Penzkofer A, Procházka R, Shen Z, Strauss J, Daub J. Absorption and emission spectroscopic characterisation of a pyrene-flavin dyad. Chem Phys 2007;331:427–37. https://doi.org/10.1016/j.chemphys.2006.11.014.
[20] Shen Z, Procházka R, Daub J, Fritz N, Acar N, Schneider S. Towards modelling light processes of blue-light photoreceptors, Pyrene-isoalloxazine (flavin)-phenothiazine triad: electrochemical, photophysical, investigations and quantum chemical calculations. Phys Chem Chem Phys 2003;5:3257–69. https://doi.org/10.1039/B301279D.
[21] Shen Z, Strauss J, Daub J. Mimicking dye-based functions of natural blue-light photoreceptors by studying photoinduced energy and electron transfer in a pyrene-isoalloxazine(flavin)-phenothiazine triad. Chem Commun (J Chem Soc Sect D) 2002:460–1. https://doi.org/10.1039/B109151D.
[22] Yu X, Eymur S, Singh V, Yang B, Tonga M, Bheemaraju A, Cooke G, Subramani C, Venkataraman D, Stanley RJ, Rotello VM. Flavin as a photo-active acceptor for efficient energy and charge transfer in a model donor–acceptor system. Phys Chem Chem Phys 2012;14:6749–54. https://doi.org/10.1039/C2CP40073A.
[23] Accorsi G, Barigelletti F, Farrán A, Herranz F, Claramunt RM, Marcaccio M, Valenti G, Paolucci F, Pinilla E, Torres MR. Intramolecular interactions and photoinduced electron transfer in isoalloxazine-naphthalene bichromophores. J Photochem Photobiol, A 2009;203:166–76. https://doi.org/10.1016/j.jphotochem.2009.01.012.
[24] Pauszek RF, Kodali G, Caldwell ST, Fitzpatrick B, Zainalabdeen NY, Cooke G, Rotello VM, Stanley RJ. Excited state charge redistribution and dynamics in the donor-π-acceptor flavin derivative ABFL. J Phys Chem B 2013;117:15684–94. https://doi.org/10.1021/jp406420h.
[25] Murakami M, Ohkubo K, Fukuzumi S. Inter- and intramolecular photoinduced electron transfer of flavin derivatives with extremely small reorganization energies. Chem Eur J 2010;16:7820–32. https://doi.org/10.1002/chem.200903236.
[26] Farrán A, Mohanraj J, Clarkson GJ, Claramunt RM, Herranz F, Accorsi G. Tuning photoinduced processes of covalently bound isoalloxazine and anthraquinone bichromophores. Photochem Photobiol Sci 2013;12:813–22. https://doi.org/10.1039/C3PP25321J.
[27] Farrán MA, Listorti A, Roiati V, Accorsi G, Gigli G, Clarkson GJ, Claramunt RM. Photoinduced processes in macrocyclic isoalloxazine-anthracene systems. J Photochem Photobiol, A 2016;314:189–97. https://doi.org/10.1016/j.jphotochem.2015.08.021.
[28] Mouli MSSV, Mishra AK. Synthesis, characterization and photophysical studies of the flavopeptide conjugates as model for the covalently linked flavoenzymes. J Chem Sci 2022;134:59. https://doi.org/10.1007/s12039-022-02050-4.
[29] Mouli MSSV, Agrawal HG, Tamrakar A, Tripathy SR, Pandey MD, Mishra AK. Investigating the spectral and electrochemical properties of novel flavin-pyrene dyads separated via variable spacer. Luminescence 2022. https://doi.org/10.1002/bio.4339.
[30] Kondo M, Nappa J, Ronayne KL, Stelling AL, Tonge PJ, Meech SR. Ultrafast vibrational spectroscopy of the flavin chromophore. J Phys Chem B 2006;110:20107–10. https://doi.org/10.1021/jp0650735.
[31] Li G, Sichula V, Glusac KD. Role of adenine in thymine-dimer repair by reduced flavin-adenine dinucleotide. J Phys Chem B 2008;112:10758–64. https://doi.org/10.1021/jp804506t.
[32] Li G, Glusac KD. Light-Triggered proton and electron transfer in flavin cofactors. J Phys Chem A 2008;112:4573–83. https://doi.org/10.1021/jp7117218.
[33] Rhee H-W, Choi H-Y, Han K, Hong J-I. Selective fluorescent detection of flavin adenine dinucleotide in human eosinophils by using bis(Zn^{2+}-dipicolylamine) complex. J Am Chem Soc 2007;129:4524–5. https://doi.org/10.1021/ja070026r.
[34] Yan L, Fu L, Li M, Bai X, Jin L. Fabrication of dual-stimuli responsive films assembled by flavin mononucleotide and layered double hydroxides. Chem Commun 2018;54:12590–3. https://doi.org/10.1039/C8CC06459H.
[35] Liu Y, Li P, Ma H, Zhang M, Li F. Fluorescent/laser dual-channel ATP sensors based on flavins. RSC Adv 2015;5:11942–5. https://doi.org/10.1039/C4RA16022C.
[36] Hong K-I, Lee SM, Jang W-D. Flavin-based light-driven fluorescent probe for the detection of antioxidant amino acids. ChemistryOpen 2018;7:57–60. https://doi.org/10.1002/open.201700144.
[37] Iida H, Miki M, Iwahana S, Yashima E. Riboflavin-based fluorogenic sensor for chemo- and enantioselective detection of amine vapors. Chem Eur J 2014;20:4257–62. https://doi.org/10.1002/chem.201400234.
[38] Mouli MSSV, Mishra AK. Formation of the silver–flavin coordination polymers and their morphological studies. CrystEngComm 2022;24:2221–5. https://doi.org/10.1039/D2CE00071G.
[39] Mouli MSSV, Mishra AK. Modulating catalytic activity of a modified flavin analogue via judicially positioned metal ion toward aerobic sulphoxidation. RSC Adv 2022;12:3990–5. https://doi.org/10.1039/D1RA06558K.
[40] Mouli MSSV, Katyal S, Mishra AK. Design and synthesis of a flavin–samarium complex as an efficient photocatalyst for sulfoxidation reactions. Synlett 2022. https://doi.org/10.1055/a-1928-3417.
[41] (d) Mouli MSSV, Mishra AK. Divergent crystallographic architecture for silver-flavin complexes induced via pH variation. ChemistrySelect 2022. https://doi.org/10.1002/slct.202202126.
[42] Vallee BL, Falchuk KH. The biochemical basis of zinc physiology. Physiol Rev 1993;73:79–118. https://doi.org/10.1152/physrev.1993.73.1.79.

[43] Maret W, Krezel A. Cellular zinc and redox buffering capacity of metallothionein/thionein in health and disease. Mol Med 2007;13:371–5. https://doi.org/10.2119/2007-00036.Maret.
[44] Li Y, Hough CJ, Frederickson CJ, Sarvey JM. Induction of mossy Fiber→CA3 long-term potentiation requires translocation of synaptically released Zn^{2+}. J Neurosci 2001;21:8015–25. https://doi.org/10.1523/JNEUROSCI.21-20-08015.2001.
[45] Sensi SL, Yin HZ, Weiss JH. AMPA/kainate receptor-triggered Zn^{2+} entry into cortical neurons induces mitochondrial Zn^{2+} uptake and persistent mitochondrial dysfunction. Eur J Neurosci 2000;12:3813–8. https://doi.org/10.1046/j.1460-9568.2000.00277.x.
[46] Frederickson CJ, Koh J-Y, Bush AI. The neurobiology of zinc in health and disease. Nat Rev Neurosci 2005;6:449–62. https://doi.org/10.1038/nrn1671.
[47] Takeda A, Tamano H. Insight into zinc signaling from dietary zinc deficiency. Brain Res Rev 2009;62:33–4. https://doi.org/10.1016/j.brainresrev.2009.09.003.
[48] Sensi SL, Paoletti P, Bush AI, Sekler I. Zinc in the physiology and pathology of the CNS. Nat Rev Neurosci 2009;10:780–91. https://doi.org/10.1038/nrn2734.
[49] Taylor CG. Zinc, the pancreas, and diabetes: insights from rodent studies and future directions. Biometals 2005;18:305–12. https://doi.org/10.1007/s10534-005-3686-x.
[50] Jansen J, Karges W, Rink L. Zinc and diabetes-clinical links and molecular mechanisms. J Nutr Biochem 2009;20:399–417. https://doi.org/10.1016/j.jnutbio.2009.01.009.
[51] Wijesekara N, Chimienti F, Wheeler MB. Zinc, a regulator of islet function and glucose homeostasis. Obes Metabol 2009;11:202–14. https://doi.org/10.1111/j.1463-1326.2009.01110.x.
[52] Costello LC, Franklin RB. Prostatic fluid electrolyte composition for the screening of prostate cancer: a potential solution to a major problem. Prostate Cancer Prostatic Dis 2009;12:17–24. https://doi.org/10.1038/pcan.2008.19.
[53] Franklin RB, Costello LC. Zinc as an anti-tumor agent in prostate cancer and in other cancers. Arch Biochem Biophys 2007;463:211–7. https://doi.org/10.1016/j.abb.2007.02.033.
[54] Costello LC, Franklin RB. The clinical relevance of the metabolism of prostate cancer; zinc and tumor suppression: connecting the dots. Mol Cancer 2006;5:17. https://doi.org/10.1186/1476-4598-5-17.
[55] Wongkongkatep J, Ojida A, Hamachi I. Fluorescence sensing of inorganic phosphate and pyrophosphate using small molecular sensors and their applications. Top Curr Chem 2017;375:30. https://doi.org/10.1007/978-3-319-60357-5_1.
[56] Ngo HT, Liu X, Jolliffe KA. Anion recognition and sensing with Zn(II)–dipicolylamine complexes. Chem Soc Rev 2012;41:4928–65. https://doi.org/10.1039/C2CS35087D.
[57] Lee H-J, Cho C-W, Seo H, Singha S, Jun YW, Lee K-H, Jung Y, Kim K-T, Park S, Baed SC, Ahn KH. A two-photon fluorescent probe for lysosomal zinc ions. Chem Commun 2016;52:124–7. https://doi.org/10.1039/C5CC06976A.
[58] Villabona-Monsalve JP, Varnavski O, Palfey BA, Goodson T. Two-Photon excitation of flavins and flavoproteins with classical and quantum light. J Am Chem Soc 2018;140:14562–6. https://doi.org/10.1021/jacs.8b08515.
[59] Kobayashi H, Katano K, Hashimoto T, Hayashita T. Solvent effect on the fluorescence response of hydroxycoumarin bearing a dipicolylamine binding site to metal ions. Anal Sci 2014;30:1045–50. https://doi.org/10.2116/analsci.30.1045.
[60] Kowser Z, Tomiyasu H, Jiang X, Rayhan U, Redshaw C, Yamato T. Solvent effect and fluorescence response of the 7-tert-butylpyrene-dipicolylamine linkage for the selective and sensitive response toward Zn^{2+} and Cd^{2+} ions. New J Chem 2015;39:4055–62. https://doi.org/10.1039/C4NJ02363C.
[61] Taki M, Wolford JL, O'Halloran TV. Emission ratiometric imaging of intracellular zinc: design of a benzoxazole fluorescent sensor and its application in two-photon microscopy. J Am Chem Soc 2004;126:712–3. https://doi.org/10.1021/ja039073j.
[62] Komatsu K, Urano Y, Kojima H, Nagano T. Development of an iminocoumarin-based zinc sensor suitable for ratiometric fluorescence imaging of neuronal zinc. J Am Chem Soc 2007;129:13447–54. https://doi.org/10.1021/ja072432g.
[63] Liu X, Wang P, Fu J, Yao K, Xue K, Xu K. Turn-on fluorescent sensor for Zinc and Cadmium ions based on quinolone and its sequential response to phosphate. J Lumin 2017;186:16–22. https://doi.org/10.1016/j.jlumin.2017.01.037.
[64] Yao P-S, Liu Z, Ge J-Z, Chen Y, Cao Q-Y. A novel polynorbornene-based chemosensor for the fluorescence sensing of Zn^{2+} and Cd^{2+} and subsequent detection of pyrophosphate in aqueous solutions. Dalton Trans 2015;44:7470–6. https://doi.org/10.1039/C5DT00542F.
[65] Singh R, Gogoi A, Das G. Benzothiazole based multi-analyte sensor for selective sensing of Zn^{2+} and Cd^{2+} and subsequent sensing of inorganic phosphates (Pi) in mixed aqueous medium. RSC Adv 2016;6:112246–52. https://doi.org/10.1039/C6RA22840B.
[66] Benesi HA, Hildebrand JH. A spectrophotometric investigation of the interaction of iodine with aromatic hydrocarbons. J Am Chem Soc 1949;71:2703–7. https://doi.org/10.1021/ja01176a030.
[67] Li Y, Wu J, Jin X, Wang J, Han S, Wu W, Xu J, Liu W, Yao X, Tang Y. A bimodal multianalyte simple molecule chemosensor for Mg^{2+}, Zn^{2+}, and Co^{2+}. Dalton Trans 2014;43:1881–7. https://doi.org/10.1039/C3DT52618F.
[68] Wan J, Duan W, Chen K, Tao Y, Dang J, Zeng K, Ge Y, Wu J, Liu D. Selective and sensitive detection of Zn(II) ion using a simple peptide-based sensor. Sensor Actuator B Chem 2018;255:49–56. https://doi.org/10.1016/j.snb.2017.08.038.
[69] Waheed A, Ahmad T, Haroon M, Ullah N. A highly sensitive and selective fluorescent sensor for zinc(II) ions based on a 1,2,3-triazolyl-functionalized 2,2'-dipicolylamine (DPA). ChemistrySelect 2020;5:5300–5. https://doi.org/10.1002/slct.202000928.
[70] Chang CJ, Jaworski J, Nolan EM, Sheng M, Lippard SJ. A tautomeric zinc sensor for ratiometric fluorescence imaging: application to nitric oxide-induced release of intracellular zinc. Proc Natl Acad Sci USA 2004;101:1129–34. https://doi.org/10.1073/pnas.0308079100.
[71] Xue L, Li G, Yu C, Jiang H. A ratiometric and targetable fluorescent sensor for quantification of mitochondrial zinc ions. Chem Eur J 2012;18:1050–4. https://doi.org/10.1002/chem.201103007.
[72] Yoon SA, Lee J, Lee MH. A ratiometric fluorescent probe for Zn^{2+} based on pyrene-appended naphthalimide-dipicolylamine. Sensor Actuator B Chem 2018;258:50–5. https://doi.org/10.1016/j.snb.2017.11.126.